Integrated Analytical Modeling to Predict Performance Characteristics of Linear Switched Reluctance Motor

Milad Golzarzadeh[a*], Zahra Nasiri-Gheidari[a], Hashem Oraee[a], Babak Ganji[b]

1- Milad Golzarzadeh

E-mail: milad.golzarzadeh@ee.sharif.edu

2- Zahra Nasiri-Gheidari

E-mail: znasiri@sharif.edu

3- Hashem Oraee

E-mail: oraee@sharif.edu

4- Babak Ganji

E-mail: bganji@kashanu.ac.ir

a) Department of Electrical Engineering, Sharif University of Technology, Tehran, Iran

b) Faculty of Electrical and Computer Engineering, University of Kashan, Kashan, Iran

---

[*]Corresponding author: Milad Golzarzadeh

E-mail: milad.golzarzadeh@ee.sharif.edu

***Abstract*—**Switched Reluctance Motors (SRMs) are classified into two types, rotary and linear, based on the type of movement. The linear switched reluctance motors (LSRMs) have the same structure as rotary types and therefore they have all the advantages of SRMs. In this paper, for the LSRM, two analytical models based on field equations in electromagnetics and Magnetic Equivalent Circuit (MEC) method are presented. The static characteristic of the flux linked with a phase is predicted in the fully aligned and fully unaligned as well as intermediate positions of the mover. Then, based on the phase voltage equation, the dynamic analysis of the motor is done and the instantaneous phase current and instantaneous thrust force are determined. By applying the developed analytical models to a three-phase LSRM, the simulation results are presented and compared with those of the Finite Element Method (FEM)

for validation. The comparisons clearly show that the presented models have appropriate calculation speed and accuracy.

Keywords— Linear Switched Reluctance Motor (LSRM), Magnetic Equivalent Circuit (MEC), Analytical Model, Finite Element Method (FEM)

1. INTRODUCTION

Switched reluctance motors (SRMs) have many applications in production automation, because these motors have prominent features such as simplicity of structure, high endurance, high fault tolerance, application in harsh environments, high reliability and operation in a wide range of speeds. Therefore, in many industrial applications [1,2], electric vehicles [3,4], rail transportation [5,6] and home use [7,8] are suitable options. The linear switched reluctance motor (LSRM) has a structure similar to its rotary counterpart in terms of performance and principles, with the difference that it has linear motion instead of rotary motion. Therefore, LSRM has all the advantages of SRM. For linear applications, in the rotary SRM, motion converters are used to convert the torque into linear force, while the LSRM does not need any motion converter and the force is directly applied to the moving part. The absence of a motion converter reduces costs and the space is used optimally, so the LSRM can be used for rail transportation and home applications [9-11].

Because of the salient pole structure and non-linear behavior, it is difficult to predict the performance characteristics of SRM. In addition, the phenomenon of local saturation causes significant changes in the characteristics of this motor, so its static and dynamic parameters change non-linearly. According to these cases, predicting the exact behavior of SRM by considering the saturation phenomenon is an important issue, and by developing non-linear analytical models, the performance characteristics of the motor can be extracted [12-13]. One of the most effective analytical methods for analyzing the performance of SRMs is the magnetic equivalent circuit (MEC) model, which can predict the important characteristics of motor with considerable accuracy and speed. The MEC model has been widely used in the literature to analyze the SRMs [14-16]. In recent years, various structures have been presented for the LSRM, which by using the MEC model, different aspects of this motor such as electromagnetic design and thermal design have been investigated and static and dynamic characteristics have been predicted [17-19]. To design and analyze the electric motor and predict the parameters of motor using the FEM, it takes a lot of time if the modeling details are considered. Therefore, it is necessary to use faster methods. The analytical method can significantly reduce the calculation time.

In [20], an analytical and standard design method for the LSRM is presented, and by using the proposed analytical methods, the important characteristics of this motor are predicted. In [21], the inductance of LSRM in aligned and unaligned positions are predicted using two-dimensional field solution and Fourier series expansion. Considering that LSRMs have the same performance as rotary SRMs, it is possible to use the analytical models presented in the rotary domain by adopting appropriate transformations to predict the characteristics of linear motors. In [22], using the magnetic permeance method, an analytical model has been developed for the rotary SRM, which can only predict the flux-linkage in two positions of fully aligned and fully unaligned. The weakness of this model is the inability to predict the flux-linkage in intermediate positions. Also, due to the many assumptions for the flux path, the accuracy of model decreases for predicting the saturation phenomenon. In [23], an analytical model is presented that only predicts the flux-linkage in the fully unaligned position and cannot be a complete model. Therefore, with the aim of improving it in [24], another analytical model is presented that predicts the flux-linkage only in aligned position. These two models are not integrated, and with the aim of improving them in [25], an integrated analytical model for linear switched reluctance motor with segmental translator is presented, which has good accuracy in predicting motor characteristics.

In order to improve the analytical model in [25], an analytical model based on the magnetic equivalent circuit approach in [26] has been developed that predicts the performance characteristics of the motor with good accuracy and speed. In this model, to form the magnetic equivalent circuit, the air-gap between the stator and the moving part is divided into four different magnetic reluctances and their values are calculated using ANSYS and MATLAB software tools. Although the models introduced in [25] and [26] have acceptable accuracy and speed, some assumptions reduce the accuracy of the results. These models are proposed for the linear motor with segmented moving part, in which discrete segments are used in the moving part instead of salient poles. The space between two adjacent segments forms a trapezoidal geometry, which is considered rectangular for predicting the flux-linkage, which reduces the accuracy of predicting the dynamic characteristics of the motor. Therefore, to solve this problem, a more accurate model is developed in this paper. The important innovation of this paper is the method of predicting the flux-linkage characteristic in unaligned and aligned positions, which is developed into an integrated model using appropriate transformation.

Among the analytical models presented for LSRM, considering that the saturation phenomenon occurs in the aligned position, but there is usually no saturation in the unaligned

position, it is difficult to provide an analytical model to predict the performance characteristics of motor in intermediate positions. Therefore, in this paper, two separate models are presented to predict flux linked in aligned and unaligned positions. In the unaligned position, assuming that no saturation occurs in the motor, the motor flux-linkage is calculated using appropriate equations in electromagnetics, while in the aligned position, assuming that saturation occurs, using the MEC model, flux-linkage is predicted. Considering the unsaturated inductance, these two separate models are linked together and an accurate and fast integrated analytical model is presented for predicting the static and dynamic characteristics of LSRM. Based on this, the developed analytical models are described in Section 2. Applying the proposed model to a typical three-phase LSRM, the simulation results are presented in Section 3. Finally, the conclusion is given in Section 4.

2. DEVELLOPED MODEL

The cross-section of a studied LSRM is shown in Fig. 1. As it is clear from this figure, each slot of the stator is filled with two phase windings. For the studied motor, the stator and the mover include ten and six poles, respectively. The positions of aligned and unaligned of the sample motor for phase B are shown in Fig. 2. Since it is enough to have one phase to analyze the SRM, so only the winding of one phase is considered, which can be generalized to the three-phase motor after analysis. In the unaligned position, the reluctance of air-gap is higher than that of the aligned position. Therefore, as it is clearly seen in Fig. 2, the flux lines are more irregular in the unaligned position. By using the magnetic potential, which is a vector quantity, the magnetic field can be obtained. Therefore, if it is possible to find the magnetic potential vector for a current distribution, with a differential operation, the magnetic flux density is obtained from the magnetic potential vector.

In the parts of motor where there is air, it is difficult to calculate the performance characteristics of motor. According to Fig. 2, in the unaligned position, the magnetic flux inevitably passes through the free space between the two poles of moving part, which can be used to calculate the static characteristics of motor using the magnetic potential vector. In the unaligned position, the flux produced by the coil can be divided into two parts: one is the flux that passes through the free space between the two poles adjacent in the moving part, and the other is partial fluxes that close their path through the stator slot. Therefore, the motor flux-linkage in the unaligned position is calculated using prediction of the fields in the air-gap between the translator poles and stator slot. In the aligned position, a simple and accurate MEC model is used to predict the motor flux-linkage.

2. 1. Unaligned Position

By applying the current to phase B, in the unaligned position of Fig. 2b, for the generated flux, the contribution of moving part and stator slot are predicted separately, then by adding these two values, the total flux in the unaligned position is obtained.

2. 1. 1. Contribution of Moving Part:

Assuming that the current is in the Z-direction, since the magnetic potential vector is generated in the direction of current, this vector is non-zero only in the Z-direction. Therefore, Poisson's equation can be written as follows:

$$\nabla^2 \mathrm{A}_z = -\mu_0 J_z \qquad (1)$$

Where A is the magnetic potential vector, μ_0 is the magnetic permeability of air and J is the electric current density. There is no current between the poles of moving part, so $J_z = 0$ and Eq. (1) reduces to Laplace's equation:

$$\nabla^2 \mathrm{A}_z = 0 \qquad (2)$$

By solving the two-dimensional equation of Laplace on the free space between the two poles of moving part in the unaligned position, the field is obtained and as a result the magnetic flux density is obtained. Then, by choosing a suitable surface and integrating on this surface, the flux-linkage is calculated. The parameters required for calculations are shown in Fig. 3. The parameters w_{tr1} and w_{tr2} are equal in the full unaligned position, which changes their value when the translator is moved.

Using the boundary conditions of the stationary magnetic field, following equation is obtained:

$$\mathrm{H}_{2t} - \mathrm{H}_{1t} = J_s \qquad (3)$$

In the yellow rectangular geometry of Fig. 3, there is no current, that is, $J_s = 0$. As a result, the tangential field in two adjacent environments are equal ($\mathrm{H}_{2t} = \mathrm{H}_{1t}$), and by having the field in one of the environments, the field in the other can be obtained. In the unaligned position, the magnetic permeability coefficient of the sheets is assumed to be almost infinite. Therefore, the tangential field at the boundary between the poles and free space as well as the lower boundary are zero and the tangential field at the upper boundary of this area is non-zero. The boundary

conditions are applied in the rectangular geometry of free space between the two poles of the moving part as shown in Fig. 4.

The y component of magnetic field denoted by H_y at $x=0$ and $x=w_{\mathrm{tr}}$_and the x component of magnetic field denoted by H_x are zero at the lower boundary, but the H_x field in the upper boundary is non-zero and unknown. The boundary conditions of the magnetic field should be converted to appropriate boundary conditions to obtain the magnetic potential vector according to Fig. 5. Therefore, by solving the Laplace's equation with appropriate boundary conditions in Fig. 5, using the separation of variables method, the magnetic potential vector is obtained as follows:

$$\mathrm{A}_z\left(x,y\right)=\sum_{k=0}^{\infty}A_{trk}\left(\cosh\left(\frac{k\pi}{w_{tr}}y\right).\cos\left(\frac{k\pi}{w_{tr}}x\right)\right) \tag{4}$$

If H_{tr} is the contribution of field in the moving part, it is calculated from the following equation:

$$\mathrm{H}_{tr}=\frac{1}{\mu_0}\left(\nabla\times\mathrm{A}_z\right) \tag{5}$$

According to (4) and (5) can be written:

$$\mathrm{H}_{tr}\left(x,y\right)=\sum_{k=0}^{\infty}A_{trk}\frac{k\pi}{w_{tr}\mu_0}\left\{\mathrm{i}_x\sinh\left(\frac{k\pi}{w_{tr}}y\right)\cos\left(\frac{k\pi}{w_{tr}}x\right)+\mathrm{i}_y\cosh\left(\frac{k\pi}{w_{tr}}y\right)\sin\left(\frac{k\pi}{w_{tr}}x\right)\right\} \tag{6}$$

In Eq. (6), by obtaining A_{trk}, the moving part field is obtained in the unaligned position. In Fig. 3, in $y=h_{tr}$, only the x component of H_{tr} can be calculated. Therefore, to obtain the approximate value of H_x at $y=h_{tr}$ where it overlaps with the stator pole, H_x becomes zero and assuming that the field in x-direction (H_x) is constant, Ampere's law is used to calculate this constant value. According to these explanations, if N is the turns per phase and I is the phase current, the following equations are written from Fig. 6:

For $0<x<w_{tr1}$:

$$\mathrm{H}_x\left(x,h_{tr}\right)=-\frac{NI}{w_{tr1}} \tag{7}$$

For $w_{tr1}<x<w_{tr1}+w_{ps}$:

$$\mathrm{H}_x\left(x,h_{tr}\right)=0 \tag{8}$$

For $w_{tr1}+w_{ps}<x<w_{tr1}+w_{ps}+w_{tr2}$:

$$\mathrm{H}_x\left(x,h_{tr}\right)=\frac{NI}{w_{tr2}} \tag{9}$$

To calculate the A_{trk} coefficient in $y=h_{tr}$, only the x-component of Eq. (6) is considered. Therefore, A_{trk} is calculated using the Fourier series as follows:

$$A_{trk}=\frac{2NIw_{tr}\mu_0}{\left(k\pi\right)^2\sinh\left(\frac{k\pi}{w_{tr}}y\right)}\times\left\{\frac{\sin\left(\frac{k\pi}{w_{tr}}q_1\right)-\sin\left(\frac{k\pi}{w_{tr}}q_2\right)}{w_{tr2}}-\frac{\sin\left(\frac{k\pi}{w_{tr}}w_{tr1}\right)}{w_{tr1}}\right\} \tag{10}$$

where:

$$q_1=w_{tr1}+w_{ts}+w_{tr2} \tag{11}$$

$$q_2=w_{tr1}+w_{ts} \tag{12}$$

By obtaining A_{trk}, the magnetic field can be calculated according to Eq. (6) in the moving section. By multiplying the H_x and H_y fields by the magnetic permeability coefficient of free space (μ_0), the magnetic flux density in the x and y direction is obtained as:

$$B_x\left(x,y\right)=\sum_{k=1}^{\infty}\frac{2NI\mu_0}{k\pi}\times\cos\left(\frac{k\pi}{w_{tr}}x\right)\times\left\{\frac{\sin\left(\frac{k\pi}{w_{tr}}q_1\right)-\sin\left(\frac{k\pi}{w_{tr}}q_2\right)}{w_{tr2}}-\frac{\sin\left(\frac{k\pi}{w_{tr}}w_{tr1}\right)}{w_{tr1}}\right\} \tag{13}$$

$$B_y\left(x,y\right)=\sum_{k=1}^{\infty}\frac{2NI\mu_0}{k\pi\tanh\left(\frac{k\pi}{w_{tr}}y\right)}\times\sin\left(\frac{k\pi}{w_{tr}}x\right)\times\left\{\frac{\sin\left(\frac{k\pi}{w_{tr}}q_1\right)-\sin\left(\frac{k\pi}{w_{tr}}q_2\right)}{w_{tr2}}-\frac{\sin\left(\frac{k\pi}{w_{tr}}w_{tr1}\right)}{w_{tr1}}\right\}$$

(14)

where $B_x(x,y)$ and $B_y(x,y)$ are the magnetic flux density of the free space between the two poles of moving part in x- and y-directions, respectively. In this area, the direction of flux is in the direction of both vertical axis and the horizontal axis. Therefore, $B_x(x,y)$ and $B_y(x,y)$ are required to obtain the magnetic flux. If n is a normal vector, the magnetic flux in x- and y-directions can be obtained by choosing the appropriate surface from the following equations:

$$\varphi = \int \mathrm{B}.nds \Rightarrow$$

$$\varphi_y = -\int \mathrm{B}.\mathrm{i}_y.ds \Rightarrow \varphi_y = -\int \mathrm{B}_y.ds \tag{15}$$

$$\varphi_x = \int \mathrm{B}.\mathrm{i}_x.ds \Rightarrow \varphi_y = \int \mathrm{B}_x.ds \tag{16}$$

Considering that the normal vectors are in the opposite direction along the horizontal axis, their sum is zero. Therefore, only the flux along the vertical axis is considered. If L_{stk} is the axial length of the motor, having the number of turns, the contribution of translator flux-linkage (λ_{tr}) of each phase is obtained as follows:

$$\lambda_{tr} = \sum_{k=1}^{\infty} -\frac{2N^2 I \mu_0 L_{stk} w_{tr}}{(k\pi)^2 \tanh\left(\frac{k\pi}{w_{tr}} y\right)} \left(1-\cos\left(\frac{k\pi}{w_{tr}} w_{ts}\right)\right) \times \left\{ \frac{\sin\left(\frac{k\pi}{w_{tr}} q_1\right) - \sin\left(\frac{k\pi}{w_{tr}} q_2\right)}{w_{tr2}} - \frac{\sin\left(\frac{k\pi}{w_{tr}} w_{tr1}\right)}{w_{tr1}} \right\} \tag{17}$$

2. 1. 2. Contribution of Stator Slot:

In unaligned position due to high air-gap reluctance, part of flux passes through the stator slot, which is difficult to calculate. In Fig. 7, assuming that the current in the stator slot conductors has a uniform distribution and the flux path is straight, the magnetic resistance of core is ignored. A strip with a width of dx, which is located at a distance x from the bottom of slot, is considered and the magnetic conductivity is calculated for two sections of the stator slot with height h_1 and h_2, then the contribution of stator slot flux-linkage is calculated through the magnetic conductivity. According to Fig. 7, the magnetic conductivity is obtained from the following equation:

$$\Lambda = \mu_0 L_{stk} \int_0^{h_1} \left(\frac{N_x}{N} \right)^2 \frac{dx}{w_s} \tag{18}$$

where:

$$\frac{N_x}{N} = \frac{w_s x}{w_s h_1} \tag{19}$$

From Eq. (18) and Eq. (19), the flux-leakage in the first and second sections are predicted from the following equations, respectively:

$$\lambda_{1s} = N^2 I \mu_0 L_{stk} \frac{h_1}{3w_s} \tag{20}$$

$$\lambda_{1s} = N^2 I \mu_0 L_{stk} \frac{h_2}{w_s} \tag{21}$$

The total flux in the stator slot is equal to the sum of flux-leakage calculated for two sections:

$$\lambda_s = \lambda_{1s} + \lambda_{2s} \tag{22}$$

From Eq. (17) and Eq. (22) the flux-linkage in unaligned position is calculated from the following equation:

$$\lambda_{unaligned} = \lambda_s + \lambda_{tr} \tag{23}$$

2. 2. Aligned Position

For the aligned position with the excitation of phase B according to Fig. 8, part of the flux generated by winding passes through the translator pole and another part passes through the free space between the two poles of translator, which are indicated by λ_m and λ_f, respectively. Therefore, to model the flux-linkage at intermediate positions, the flux path width is divided into two separate parts. These two parameters are variable so that with the displacement of the moving part, their values change and an increase in one causes a decrease in the other. At the beginning of aligned position, all the flux produced by a phase closes its path through the air-gap between the two poles of translator. Therefore, $\lambda_m = 0$. Also, in the fully aligned position according to Fig. 2a, the produced flux closes its path through the translator pole, hence $\lambda_f = 0$. To calculate the flux-linkage in aligned position, an accurate MEC model is presented in this subsection. The proposed MEC model predicts the magnetic saturation in the aligned position with high accuracy, then λ_m and λ_f can be calculated.

2. 2. 1. Prediction of λ_m :

By exciting the phase B in LSRM, the magnetic flux lines for the fully aligned position are obtained by the two-dimensional FEM using ANSYS software and can be seen in Fig. 9. According to the flux path in this figure, the MEC model for the LSRM is suggested according to Fig. 10. Using Ampere's law, the equation of the magnetic motive force (MMF) according to the flux λ_m is obtained as follows:

$$NI = \left(2\mathrm{R}_{sp} + \mathrm{R}_{sy} + 2\mathrm{R}_{trp} + \mathrm{R}_{try} + 2\mathrm{R}_{g}\right)\varphi = \mathrm{R}_{t}\varphi \qquad (24)$$

In Eq. (24), R_{sp} and R_{sy} are the reluctances related to the pole and yoke of stator, R_{trp} and R_{try} are the reluctances related to pole and yoke of translator and R_{g} is the air-gap reluctance between stator and translator. In this equation, the calculation of reluctances, especially air-gap magnetic reluctances, are difficult and requires special methods that challenge the simplicity of the magnetic equivalent circuit model. To solve this problem, since the goal is to calculate the magnetic flux, all the magnetic reluctances in Fig. 10, can be written in their equivalent form.

By determining the equivalent magnetic reluctance in Eq. (24), the flux can be calculated. It is difficult to calculate these reluctances with the movement of translator. Therefore, both saturation and translator position should be entered in Eq. (24) by choosing the appropriate method. Assuming that the motor goes into saturation in the aligned position, to consider the saturation phenomenon, the B-H curve of sheets is interpolated using the following equation [27]:

$$B = \frac{\mu H_{fe}}{1 + \dfrac{\mu H_{fe}}{B_{sat}}} + \mu_0 H_{fe} \qquad (25)$$

where, the two parameters B_{sat} and μ are determined by interpolating the magnetization curve of the motor laminations with this equation. In Fig. 8, according to the flux path, the following equation is obtained:

$$2H_{fe}L + 2H_{g}L_{g} = NI \qquad (26)$$

In this equation, L is the average length of the flux path in iron, L_g is the length of the air-gap, H_{fe} and H_g are the magnetic intensity in iron and air-gap, respectively. For the air-gap, the following equation can be written:

$$B = \mu_0 H_g \tag{27}$$

From Eq. (24), Eq. (26) and Eq. (27) we can write:

$$\mathrm{R}_t \varphi = 2H_{fe} L + \frac{2L_g B}{\mu_0} \tag{28}$$

Assuming that the cross-sectional area of flux in the air-gap and the translator pole is equal to A, By multiplying the flux cross-sectional area and the magnetic flux density, the magnetic flux passing through that area is calculated. Therefore, following quadratic equation is formed from Eq. (25) and Eq. (28):

$$\varphi = \frac{A\mu\left(\frac{\mathrm{R}_t\varphi}{2L} - \frac{BL_g}{\mu_0 L}\right)}{1 + \frac{\mu\left(\frac{\mathrm{R}_t\varphi}{2L} - \frac{BL_g}{\mu_0 L}\right)}{B_{sat}}} + A\mu_0\left(\frac{\mathrm{R}_t\varphi}{2L} - \frac{BL_g}{\mu_0 L}\right) \Rightarrow$$

$$\varphi B_{sat} + \frac{\mathrm{R}_t \mu \varphi^2}{2L} - \frac{\varphi^2 \mu L_g}{A\mu_0 L} =$$

$$\frac{B_{sat} A\mu \mathrm{R}_t \varphi}{2L} - \frac{B_{sat} A\mu\varphi L_g}{A\mu_0 L} + \frac{B_{sat} A\mu_o \mathrm{R}_t \varphi}{2L} + \frac{A\mu\mu_o \mathrm{R}_t^{\,2}\varphi^2}{4L^2} - \frac{A\mu_o \mathrm{R}_t \mu L_g \varphi^2}{2A\mu_0 L^2} -$$

$$\frac{B_{sat} A\mu_o \varphi L_g}{A\mu_0 L} - \frac{A\mu_o L_g \mu \mathrm{R}_t \varphi^2}{2A\mu_0 L^2} + \frac{A\mu_o \mu L_g^{\,2}\varphi^2}{A^2 \mu_0^{\,2} L^2} \Rightarrow$$

$$\varphi^2\left(\frac{\mathrm{R}_t\mu}{2L} - \frac{\mu L_g}{A\mu_0 L} - \frac{A\mu\mu_o \mathrm{R}_t^{\,2}}{4L^2} + \frac{L_g \mu \mathrm{R}_t}{L^2} - \frac{\mu L_g^{\,2}}{A\mu_o L^2}\right)$$

$$+\varphi\left(B_{sat} - \frac{B_{sat} A\mu \mathrm{R}_t}{2L} + \frac{B_{sat}\mu L_g}{\mu_0 L} - \frac{B_{sat} A\mu_o \mathrm{R}_t}{2L} + \frac{B_{sat} L_g}{L}\right) = 0 \tag{29}$$

This equation has two separate solutions, one of which is correct considering the modeling goal. In Eq. (29), $\varphi = 0$ cannot provide the desired solution. Therefore, the acceptable answer is obtained from the following equation:

$$\varphi = -\frac{2ALB_{sat}\left(2L - A\mathrm{R}_t\left(\mu+\mu_0\right)+2L_g\left(1+\mu_r\right)\right)}{\mu \mathrm{R}_t A\left(2L - A\mu_0 \mathrm{R}_t + 4L_g\right) - 4\mu_r L_g\left(L+L_g\right)} \tag{30}$$

In Eq. (24), it is necessary to determine the equivalent magnetic reluctance to obtain the magnetic flux in different parts of the motor. For this purpose, equation Eq. (30) is used. From Eq. (24) and Eq. (30) a quadratic equation is obtained in terms of R_t which has two separate solutions. This equation and its solutions are obtained as follows:

$$\mathrm{R}_t{}^2 - \left(\frac{4ALB_{sat}\left(L+L_g\left(1+\mu_r\right)\right)+2A\mu NI\left(L+2L_g\right)}{2LB_{sat}A^2\left(\mu+\mu_0\right)+A^2\mu_0\mu NI}\right)\mathrm{R}_t + \left(\frac{4L\mu_r L_g NI - 4\mu_r g^2 NI}{2LB_{sat}A^2\left(\mu+\mu_0\right)+A^2\mu_0\mu NI}\right) = 0 \Rightarrow$$

$$\mathrm{R}_t = \frac{2LZB_{sat}+\mu NI\left(L+2L_g\right)}{2LB_{sat}A\left(\mu+\mu_0\right)+A\mu_0\mu NI} \pm \mu N \frac{\sqrt{\left(\frac{2LZB_{sat}}{\mu N}\right)^2 + \frac{4LWB_{sat}}{\mu N} I + SI^2}}{2LB_{sat}A\left(\mu+\mu_0\right)+A\mu_0\mu NI} \tag{31}$$

where

$$Z = L + L_g\left(1+\mu_r\right) \tag{32}$$

$$W = Z\left(L+2L_g\right) - 2L_g\left(1+\mu_r\right)\left(L-L_g\right) \tag{33}$$

$$S = L^2 + 8L_g{}^2 \tag{34}$$

Only one solution to this equation is acceptable. This solution is determined using the current value. In Eq. (31), for zero current, the value of R_t should not become zero. Therefore, only positive sign is considered. In Fig. 10, to predict the flux, considering both saturation phenomenon and translator position, it is difficult to calculate the reluctances, but it can be done with high accuracy using Eq. (31). By obtaining the flux from Eq. (24) and Eq. (31), it is possible to obtain the flux linked in aligned position by considering the saturation as follows:

$$\lambda_m = N\varphi \tag{35}$$

2. 2. 2. Prediction of λ_f :

Ampere's law is also valid for the closed path created by the λ_f. In the middle lengths of the aligned position where there are both λ_m and λ_f, by following the closed path of λ_f and applying Ampere's law, the following equation is written:

$$2H_{fe}L + 2H_{gf}L_{gf} = NI \qquad (36)$$

Here, the value of L_{gf} , which is the length of flux in space between the two translator poles, is different from L_g . Therefore, the magnetic field created by λ_m and λ_f are also different. As a result, the same model that was presented to predict the value of λ_m is used with simple changes to predict the λ_f . The cross-sectional area through which the λ_f passes is a part of the stator pole that does not overlap with the translator pole in the aligned position. If w_{sp} is stator pole width and w_{trp} is a variable value and equal to the part of translator pole that overlaps with the stator pole, then the width that λ_f passes through is $w_{sp} - w_{trp}$.

In the proposed model for the unaligned position, it was assumed that motor does not go to saturation, but in the model presented in the aligned position, assuming that the motor goes to saturation, a B-H curve was considered for the saturation. Therefore, these two models are independent of each other. In order to connect the two models together, unsaturated inductance is obtained near the beginning of the aligned position where λ_f has its highest value. This inductance is calculated using the proposed model for the unaligned position where the aligned position has not yet started. With the mentioned considerations, the length of path λ_f in space between the translator poles has its maximum value at the beginning of aligned position and its minimum value in the full aligned position. Therefore, this length is obtained from the following equation:

$$L_{gf} = L_g + L_{gtr}\left(1 - \frac{w_{trp}}{w_{sp}}\right) \qquad (37)$$

where length L_{gtr} is obtained from the unsaturated inductance calculated from the proposed model for the unaligned position. If L_{tr} is the unsaturated inductance, the following equation is obtained:

$$L_{gtr} = \frac{N^2 L_{stk}\left(w_{sp} - w_{trp}\right)\mu_0}{L_{tr}} - L_g \qquad (38)$$

Therefore, by applying these changes to (31), the following equation is obtained:

$$\mathrm{R}_{tf} = \frac{2B_{sat}LZ_f + \mu NI\left(L+2L_{gf}\right)}{2LB_{sat}A_f\left(\mu+\mu_0\right)+A_f\mu_0\mu NI} + \mu N\frac{\sqrt{\left(\frac{2LZ_fB_{sat}}{\mu N}\right)^2+\frac{4LW_fB_{sat}}{\mu N}I+S_fI^2}}{2LB_{sat}A_f\left(\mu+\mu_0\right)+A_f\mu_0\mu NI} \quad (39)$$

where

$$Z_f = L + L_{gf}\left(1+\mu_r\right) \quad (40)$$

$$W_f = Z_f\left(L+2L_{gf}\right)-2L_{gf}\left(1+\mu_r\right)\left(L-L_{gf}\right) \quad (41)$$

$$S_f = L^2 + 8{L_{gf}}^2 \quad (42)$$

$$A_f = L_{stk}\left(w_{sp}-w_{trp}\right) \quad (43)$$

From Eq. (24) and Eq. (39), λ_f is obtained from as follows:

$$\lambda_f = N\varphi_f \quad (44)$$

By adding Eq. (35) and Eq. (44), the phase flux-linkage in the aligned positions is predicted from the following equation:

$$\lambda_{aligned} = \lambda_m + \lambda_f \quad (45)$$

3. SIMULATION RESULTS

The simulation results based on the proposed analytical models and 2-D FEM for LSRM are given here. Motor specifications are given in Table 1 and the sheets of stator core and translator are M800-50A with a thickness of 0.5 mm. For the sample LSRM, the parameters of B_{sat} and μ are obtained from the interpolation of the B-H curve of the motor sheets with Eq. (25) 1.8 and 0.00997, respectively, and this interpolation is shown in Fig. 11. Using the analytical models and the FEM, the static characteristics of the flux-linkage with a phase of LSRM are predicted, which are shown in Fig. 12. These characteristics have been obtained by applying currents of 0 to 20 A for phase B and moving from the unaligned position to the aligned position with a length of 69 mm.

In order to better evaluate the results of analytical model and FEM, the flux-linkage obtained in the positions of fully aligned and fully unaligned as well as the middle position are compared in Fig. 13 and Table 2.These comparisons clearly show that the introduced analytical model has a suitable accuracy in predicting the static characteristic of the flux linked for all translator

positions, and due to its calculation speed, it can be properly used in the performance analysis of the three-phase LSRM.

Having the characteristic of flux-linkage (λ) for the currents and different positions, other characteristics including co-energy ($w_c\left(x,i\right)$) and static force ($F\left(x,i\right)$) can be obtained using the following equations:

$$w_c\left(x,i\right)=\int \lambda\left(x,i\right)di \tag{46}$$

$$F\left(x,i\right)=\frac{\partial w_c\left(x,i\right)}{\partial x}|_{\text{i=const}} \tag{47}$$

According to (46), the area between the aligned and unaligned graphs represents the motor energy. So, more area means more co-energy and thus more static force. The co-energy characteristics for LSRM is compared only for currents of 6, 12 and 16 A and depicted in Fig. 14. Based on Eq. (47), the force static characteristic in different positions and currents for LSRM is obtained, which is shown in Fig. 15.

In order to calculate the dynamic characteristics of LSRM, including the instantaneous phase current ($i\left(x\right)$) and the instantaneous thrust force ($F\left(x\right)$), having the flux-linkage characteristic, first the phase instantaneous current is obtained from the phase voltage equation as follows:

$$V=Ri+\frac{d\lambda\left(x,i\right)}{dt} \tag{48}$$

where R is the resistance of the phase winding and V is the phase voltage. Having ($i\left(x\right)$) and the force static characteristic ($F\left(x,i\right)$), the instantaneous thrust force ($F\left(x\right)$) is calculated. The control parameters for calculating instantaneous current and thrust force are the turn-on position (x_{on}) and the turn-off position (x_{off}) of phase. For this LSRM, x_{on} and x_{off} are considered 13.8 mm and 48.3 mm, respectively. Considering these cases, the waveforms of instantaneous current and instantaneous thrust force for LSRM are predicted and compared using the proposed analytical model and FEM, which shown in Fig. 16 and Fig. 17, respectively. The RMS value of instantaneous phase current predicted using analytical model and FEM are 8.83 and 8.97, respectively, while the average instantaneous thrust predicted using analytical model and FEM are 66.93 and 66.85, respectively. The static and dynamic comparisons of

LSRM using the developed analytical model and the FEM show that the presented model predicts the performance characteristics of motor with high speed and acceptable accuracy.

In order to better evaluate the presented analytical model, for the operating point phase voltage is 150 V and speed is 3 m/s, the instantaneous thrust force and force ripple are also calculated. For the proposed analytical model and the finite element method, turn-on position and turn-off position are considered to be equal to 18 mm and 32 mm, respectively. Considering this operating point, the instantaneous thrust force curves for two different models are shown in Fig. 18. The average instantaneous thrust force and force ripple for the proposed analytical model are obtained as 71.56 N and %61.9, respectively, while for the finite element method they are calculated as 70.7 N and %57.35, respectively, which shows that the proposed integrated analytical model has an acceptable accuracy in predicting the dynamic characteristics of the LSRM.

The finite element method (FEM) has high accuracy to predict the results and it is a conventional method for validation of the proposed analytical models. In the FEM, in order to increase the accuracy of the model, meshing details and adding appropriate boundary conditions must be considered. Therefore, although considering these details increases the accuracy of the FEM, it also increases the calculation time, while in analytical models, fewer details are considered, which reduces the accuracy of the results compared to the FEM. The main advantage of analytical methods is the time required to predict motor characteristics, which is much less than those of the FEM. To predict the characteristic of flux-linkage, the simulation time (related to a Core i3. processor speed: 2.27GHz, RAM: 4GB) is 45 seconds for the developed analytical model and 55 minutes for FEM, while in [25] is 29 seconds for proposed analytical model and 45 minutes for FEM.

To evaluate the accuracy of the analytical model presented in this paper compared to the analytical model presented in [25], the dynamic characteristics are compared with the FEM. The average thrust force and the RMS value of current for the developed model of this paper are 66.93 N and 8.83 A, respectively, while for the FEM are 66.85 N and 8.97 A, respectively. The error of the results for the average thrust force and current are %0.12 and %-1, respectively. Also, the average thrust force and RMS value of current for the proposed model in [25], are 60 N and 6.05 A, respectively, while for the FEM are 63.1 N and 6 A, respectively. The error of the results for the average thrust force and current are %-4.9 and %0.8, respectively. These results show that the accuracy of the analytical model presented in this paper for predicting motor performance characteristics is acceptable**.**

4. CONCLUSION

In this paper, two analytical models based on solution of field equations in the unaligned position and magnetic equivalent circuit model in the aligned position were presented to predict the performance characteristics of the linear switched reluctance motor in different positions of translator. Having the characteristic of flux-linkage with a phase, the dynamic characteristics of motor, including instantaneous phase current and thrust force, were calculated from the phase voltage equation. Due to the high speed (the simulation time is 45 seconds for the developed analytical model and 55 minutes for FEM) of developed model, it can be used properly for the iterative design and optimization process of the motor. The proposed models were applied to a typical three-phase linear switched reluctance motor and the simulation results were presented and compared with the results obtained from the finite element method for validation. These comparisons showed that the analytical models were highly accurate in predicting the performance characteristics of motor and due to their calculation speed, they can be properly used in the performance analysis and optimal design of the linear switched reluctance motor.

5. REFERENCES

[1] Kumar, P., Israyelu, M., Sashidhar, S. “A simple four-phase switched reluctance motor drive for ceiling fan applications”, IEEE Access, 11, pp. 7021-7030 (2023). https://doi.org/10.1109/ACCESS.2023.3238068

[2] Chaurasiya, S. K., Bhattacharya, A., Das, S. “Reduced Switch Multilevel Converter for Grid Fed SRM Drive to Improve Magnetization and Demagnetization Characteristics of an SRM”, IEEE Trans. on Ind. Appl. 59(6), pp. 6804-6816, (2023). https://doi.org/10.1109/TIA.2023.3305594

[3] Sun, X., Wan, B., Lei, G., et al. “Multiobjective and multiphysics design optimization of a switched reluctance motor for electric vehicle applications”, IEEE Trans. Energy Convers. 36(4), pp. 3294–3304 (2021). https://doi.org/10.1109/TEC.2021.3078547

[4] Upadhyay, P. and K, R. “Design of Two-Phase Switched Reluctance Motor (SRM) for Two-Wheel Electric Vehicle and Torque-Density Based Comparison With Three-Phase SRM”, IEEE Trans. Ind. Appl. 60(3), pp. 3912-3919 (2024). https://doi.org/10.1109/TIA.2024.3371394

[5] Lu, M. and Cao, R. “Comparative Investigation of High Temperature Superconducting Linear Flux-Switching Motor and High Temperature Superconducting Linear Switched Reluctance Motor for Urban Railway Transit”, IEEE Trans. Applied Supercond. 31(5), pp. 1-5, (2021). https://doi.org/10.1109/TASC.2021.3054604

[6] Prasad, N. and Bukya, M. “New transverse linear switched reluctance motor design and analysis for transit uses”, Cogent Engineering, 11(1) (2024). https://doi.org/10.1080/23311916.2024.2406378

[7] Upadhyay, P., K, R. “Design of two-phase 4/6 switched reluctance motor for bidirectional starting in washing machine application”, IEEE Trans. Ind. App. 59(2), pp. 1519-1529 (2023). https://doi.org/10.1109/TIA.2022.3221908

[8] Wang, D., Feng, Z., Zheng, H., et al. “Comparative analysis of different topologies of linear switched reluctance motor with segmented secondary for vertical actuation systems”, IEEE Trans. Energy Convers. 36(4), pp. 2634–2645 (2021). https://doi.org/10.1109/TEC.2021.3070563

[9] Masoudi, S., Mehrjerdi, H., Ghorbani, A. “New elevator system constructed by multi-translator linear switched reluctance motor with enhanced motion quality”, IET Electr. Power Appl. 14(9), pp. 1692–1701 (2020). https://doi.org/10.1049%2Fiet-epa.2019.0996

[10] Golzarzadeh, M., Oraee, H., Ganji, B. “Design and Optimization of Segmental Translator Linear Switched Reluctance Motor”, Scientia Iranica (In press), (2024). https://doi.org/10.24200/sci.2024.63851.8624

[11] Golzarzadeh M., Oraee H., Ganji B. “Modeling and analysis of segmental translator permanent magnet linear switched reluctance motor”, 2024 32nd International Conference on Electrical Engineering (ICEE), Tehran, Iran, pp. 1-6 (2024). https://doi.org/10.1109/ICEE63041.2024.10667948

[12] Nie, R., Chen, H., Zhao, W., et al. “Comparative researches on double-sided switched reluctance linear machines with different winding connections”, IET Electr. Power Appl. 14(11), pp. 2082–2091, (2020). https://doi.org/10.1049/iet-epa.2020.0072

[13] Golzarzadeh, M. Oraee, H. Ganji, B. “Improving the performance characteristics of conventional linear switched reluctance motor by eliminating translator yoke and embedding permanent magnets in stator yoke”, Journal of Applied Research in Electrical Engineering, 3(2), pp. 222-231, (2024). https://doi.org/10.22055/jaree.2024.46343.1111

[14] Chen, H., Liu, X., Yan, W. “Three-Dimensional Magnetic Equivalent Circuit Research of Double-Sided Switched Reluctance Linear Machine”, IEEE Trans. Applied Supercond., 30(4), pp. 1-8, (2020). https://doi.org/10.1109/TASC.2020.2990774

[15] Watthewaduge, G. and Bilgin, B. “Reluctance Mesh-Based Magnetic Equivalent Circuit Modeling of Switched Reluctance Motors for Static and Dynamic Analysis”, IEEE Trans. Transp. Electrific., 8(2), pp. 2164-2176, (2022). https://doi.org/10.1109/TTE.2021.3132885

[16] Ding, W., Yin, Z., Liu, L., et al. “Magnetic circuit model and finite-element analysis of a modular switched reluctance machine with e-core stators and multi-layer common rotors,” IET Elect. Power Appl., 8(8), pp. 296-309, (2014). https://doi.org/10.1049%2Fiet-epa.2013.0366

[17] Ghaffarpour, A., Vatani, M., Jalali, M. A., Mirsalim, M. “Analysis of linear permanent magnet switched reluctance motors with modular and segmental movers”, IET Electr. Power Appl. 17(6), pp. 756–772, (2023). https://doi.org/10.1049/elp2.12300

[18] Nie, R., Chen, H., Liu, J., et al. “Compensation analysis of longitudinal end effect in three-phase switched reluctance linear machines”, IET Elect. Power App., 14(2), pp.165-174, (2020). https://doi.org/10.1049/iet-epa.2019.0142

[19] Golzarzadeh, M., Oraee, H., Ganji, B. “Lumped parameter thermal model for segmental translator linear switched reluctance motor”, IET Electr. Power Appl. 17(12), pp. 1548-1561, (2023). https://doi.org/10.1049/elp2.12362

[20] Lee, B. S., Bae, H. K., Vijayraghavan, P., et al. “Design of a linear switched reluctance machine”, IEEE Trans. Ind. Appl., 36(6), pp. 1571-1580, (2000). https://doi.org/10.1109/IAS.1999.799160

[21] Jang, S. M., Park, J. H., Choi, J. Y., et al. “Analytical prediction and measurements for inductance profile of linear switched reluctance motor”, IEEE Trans. Magn., 42(10), pp. 3428-3430, (2006). https://doi.org/10.1109/TMAG.2006.879085

[22] Mao, S. H., Dorrell, D., Tsai, M. C. “Fast analytical determination of aligned and unaligned flux linkage in switched reluctance motors based on a magnetic circuit model”, IEEE Trans. Magn., 45(7), pp. 2935-2942, (2009). https://doi.org/10.1109/TMAG.2009.2016087

[23] Radun, A. “Analytical calculation of the switched reluctance motor's unaligned inductance”, IEEE Trans. Mag., 35(6), pp. 4473-4481, (1999). https://doi.org/10.1109/20.809140

[24] Radun, A. “Analytically computing the flux linked by a switched reluctance motor phase when the stator and rotor poles overlap”, IEEE Trans. Mag., 36(4), pp. 1996-2003, (2000). https://doi.org/10.1109/20.875277

[25] Golzarzadeh, M. and Ganji, B. “Analytical modelling of the linear switched reluctance motor with segmental translator”, IET Elect. Power Appl., 13(4), pp. 527-537, (2019). https://doi.org/10.1049/iet-epa.2018.5516

[26] Golzarzadeh, M., Oraee, H., Ganji, B. “A magnetic equivalent circuit model for segmental translator linear switched reluctance motor”, Computers and Electrical Engineering. vol. 121, (2025). https://doi.org/10.1016/j.compeleceng.2024.109907

Figures:

Tables:

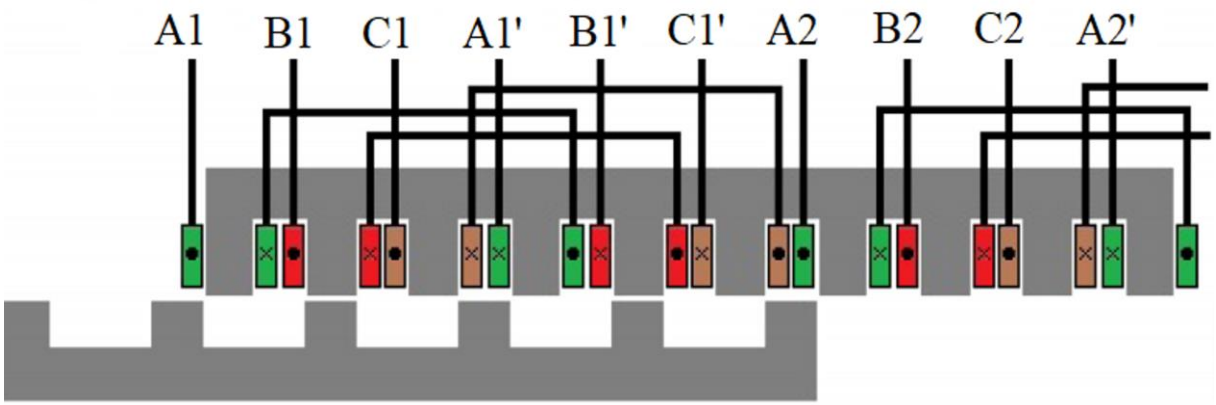

Fig. 1. The linear witched reluctance motor (LSRM) [13]

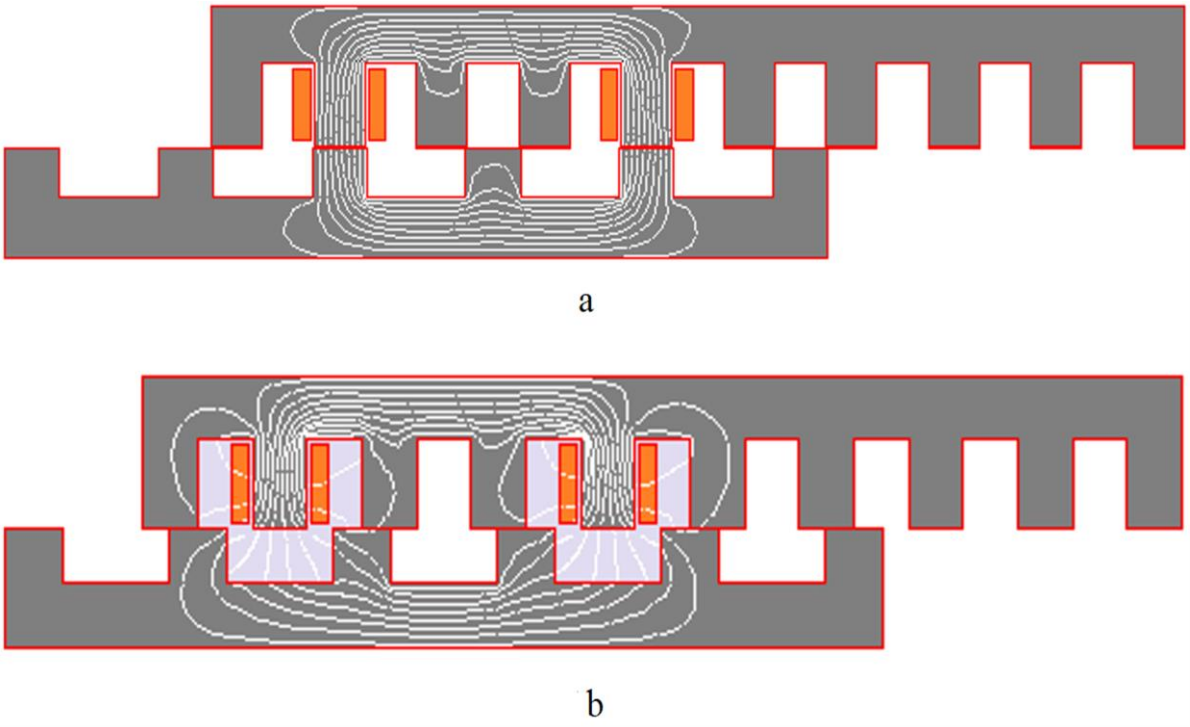

Fig. 2. Important positions for phase B: (a) Aligned, (b) Unaligned

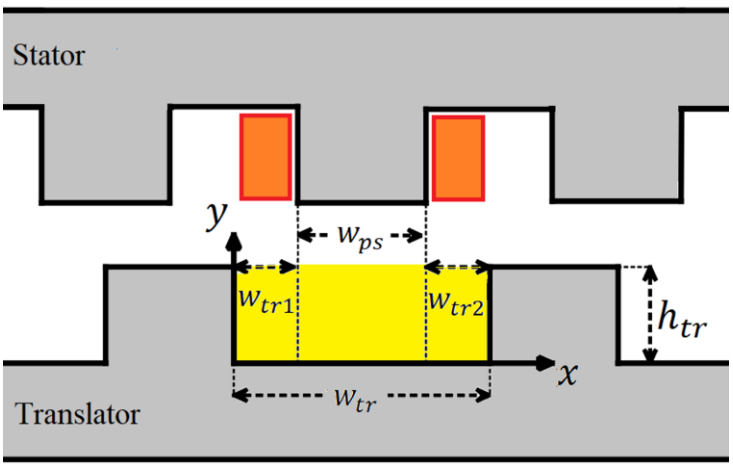

Fig. 3. Ggeometry of stator and air-gap between two poles of moving part in unaligned position

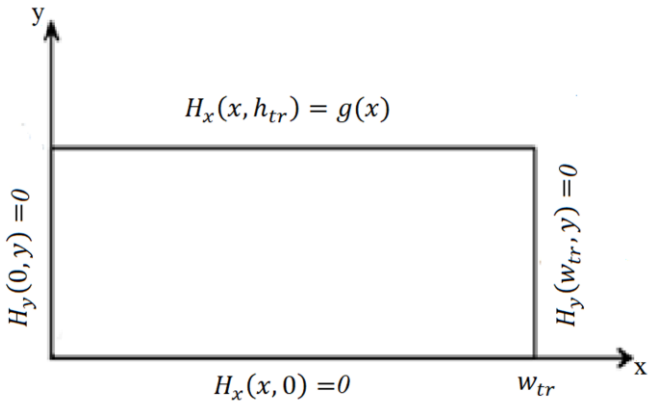

Fig. 4. Boundary conditions modeled in free space between the translator poles

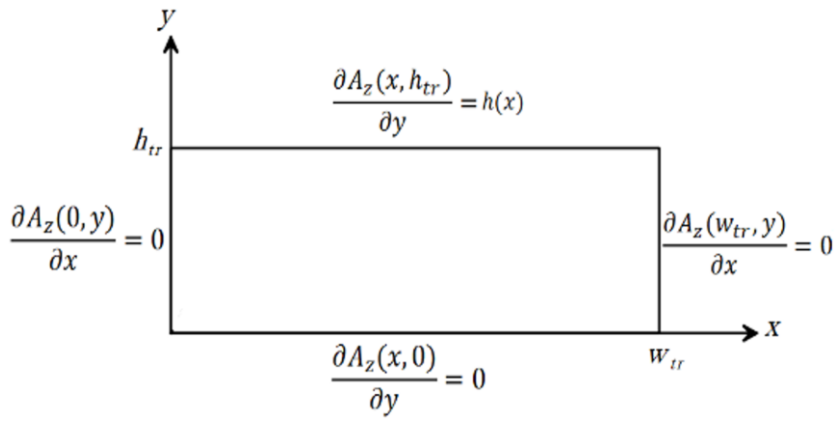

Fig. 5. Appropriate boundary conditions [25]

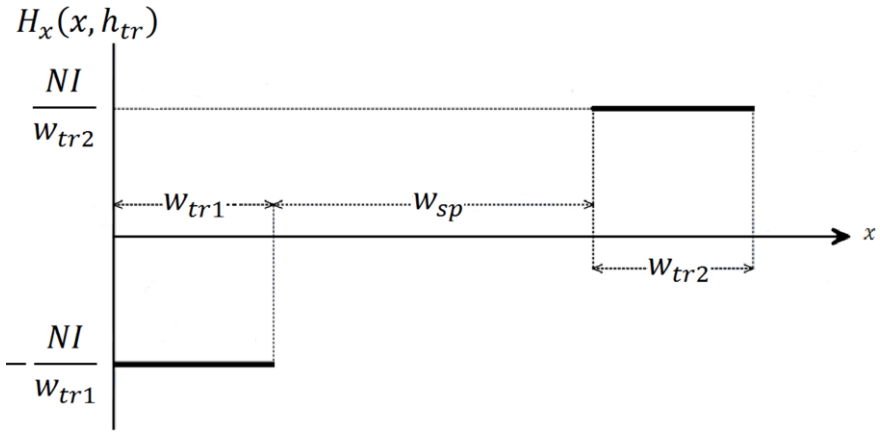

Fig. 6. Magnetic field in the x-direction at the upper boundary of air-gap between the two poles

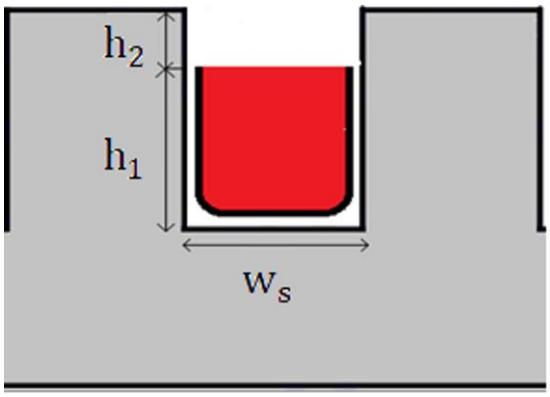

Fig. 7. Stator slot geometry to calculate stator slot flux-leakage

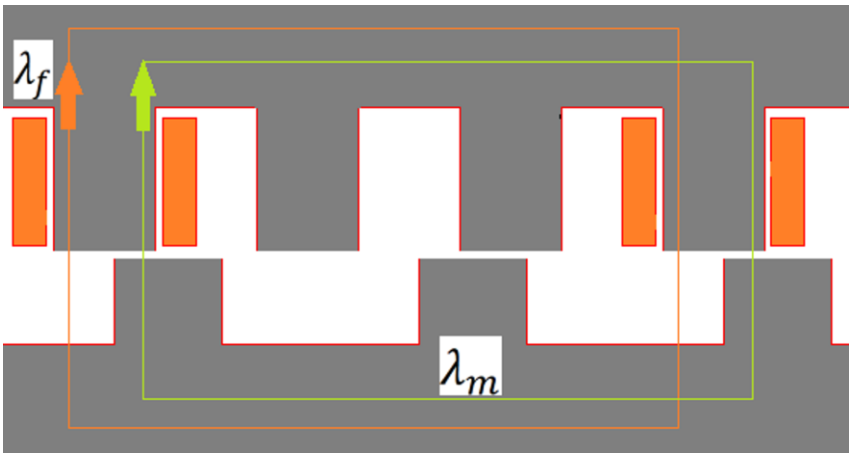

Fig. 8. Geometry of motor to calculate flux-linkage in aligned position

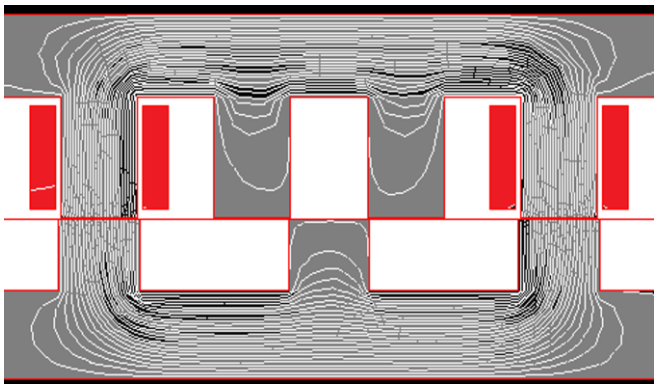

Fig. 9. Flux path in aligned position

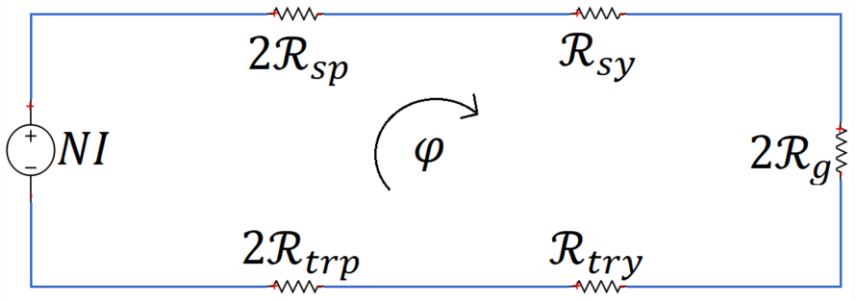

Fig. 10. The magnetic equivalent circuit corresponding to the aligned position

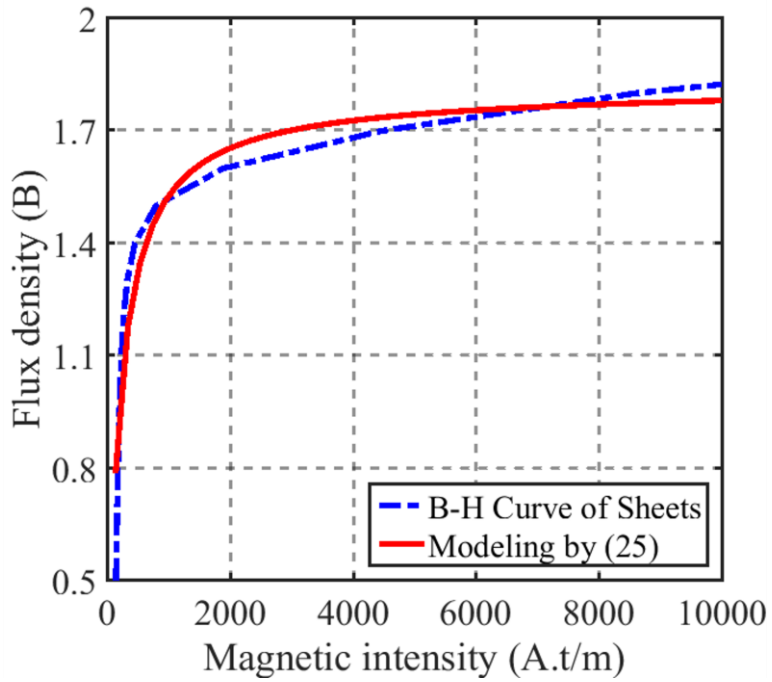

Fig. 11. Interpolation of the motor sheets B-H curve with (25)

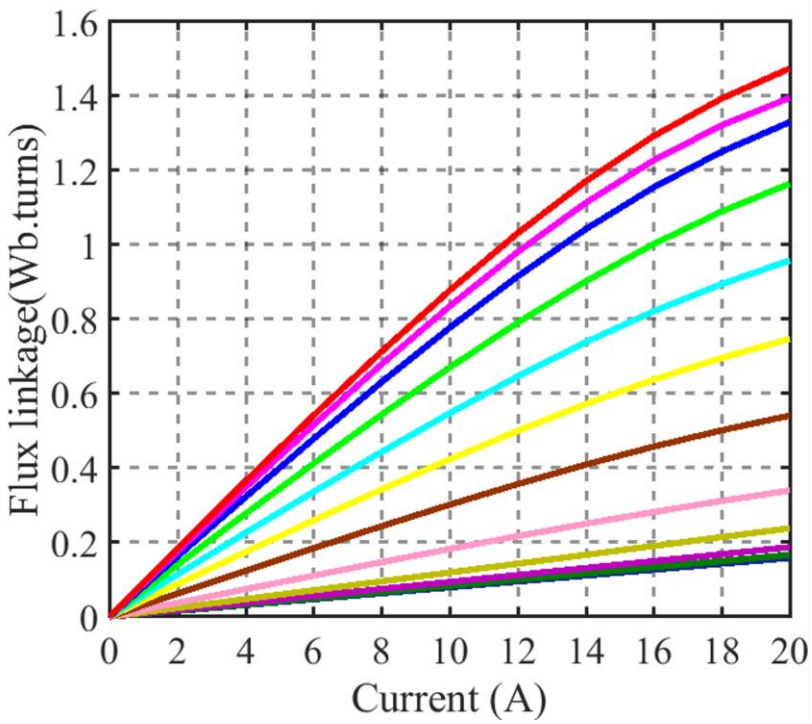

a

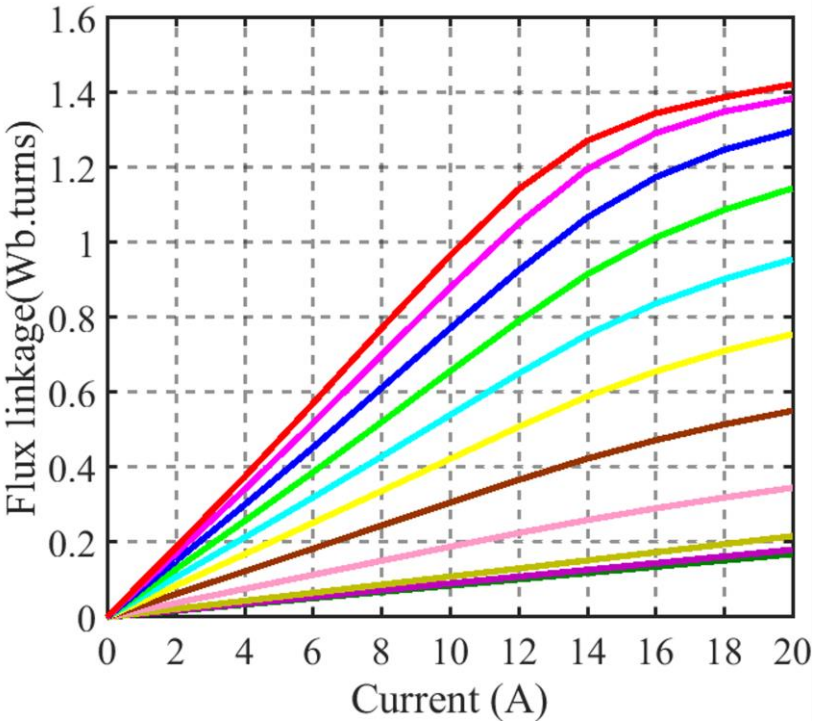

b

Fig. 12. Static characteristic of flux linked with a phase: (a) proposed analytical model, (b) FEM

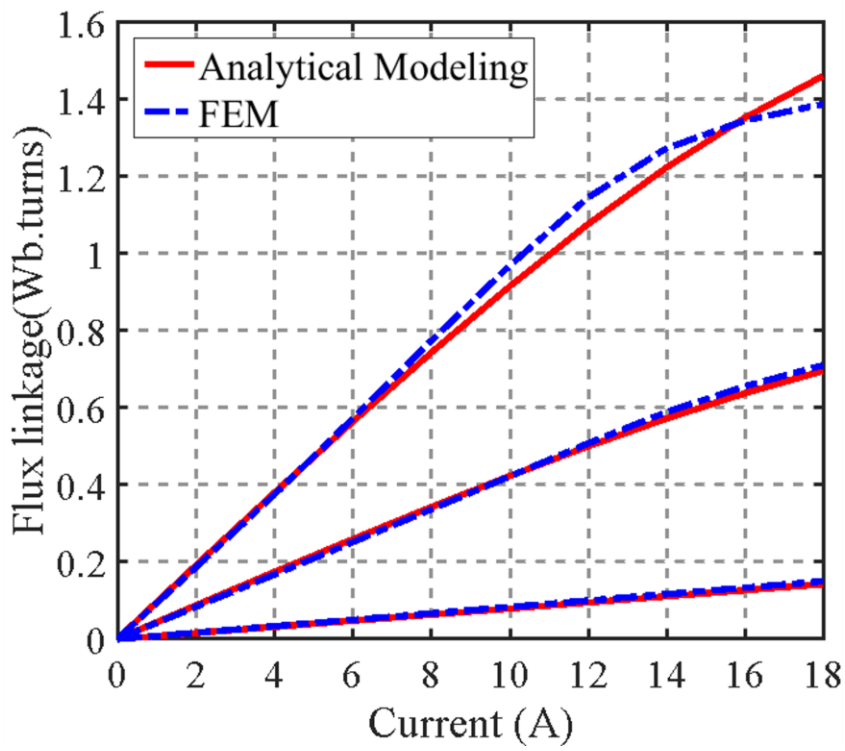

Fig. 13. Flux linked for three positions

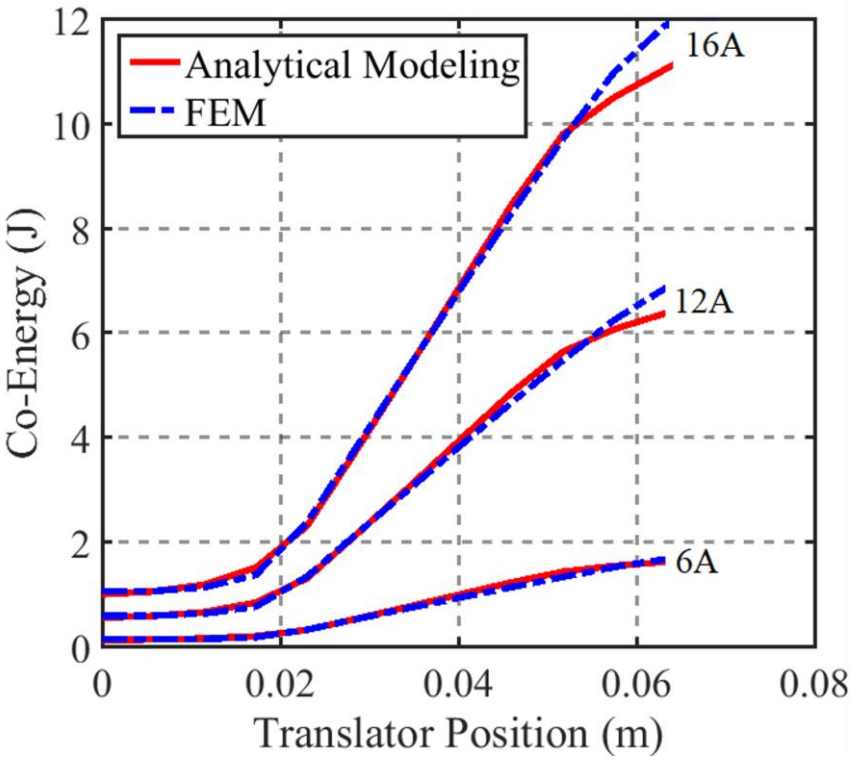

Fig. 14. Comparison of co-energy for LSRM

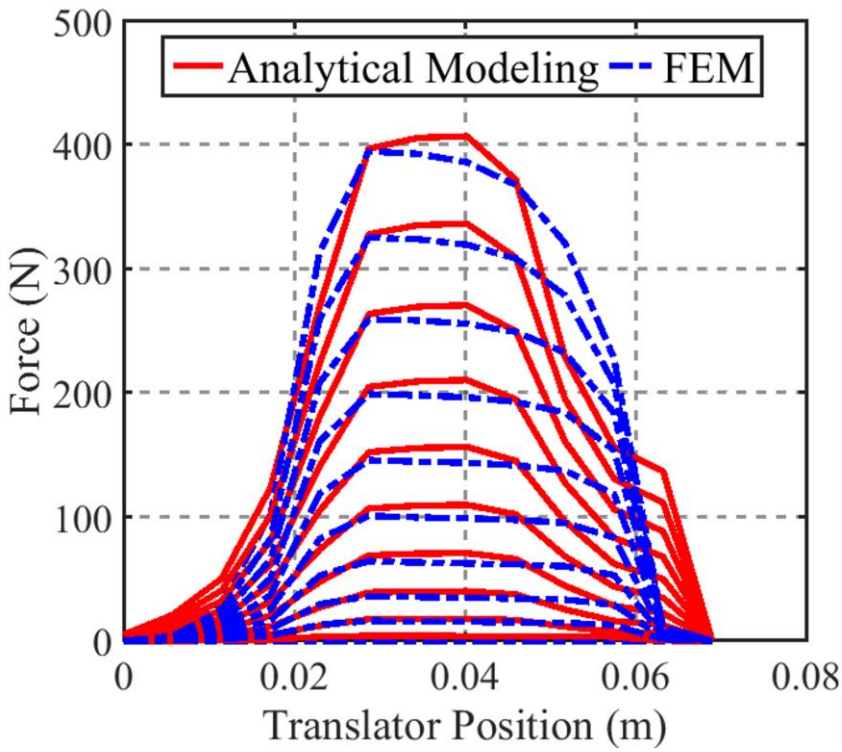

Fig. 15. Characteristic of static force for LSRM

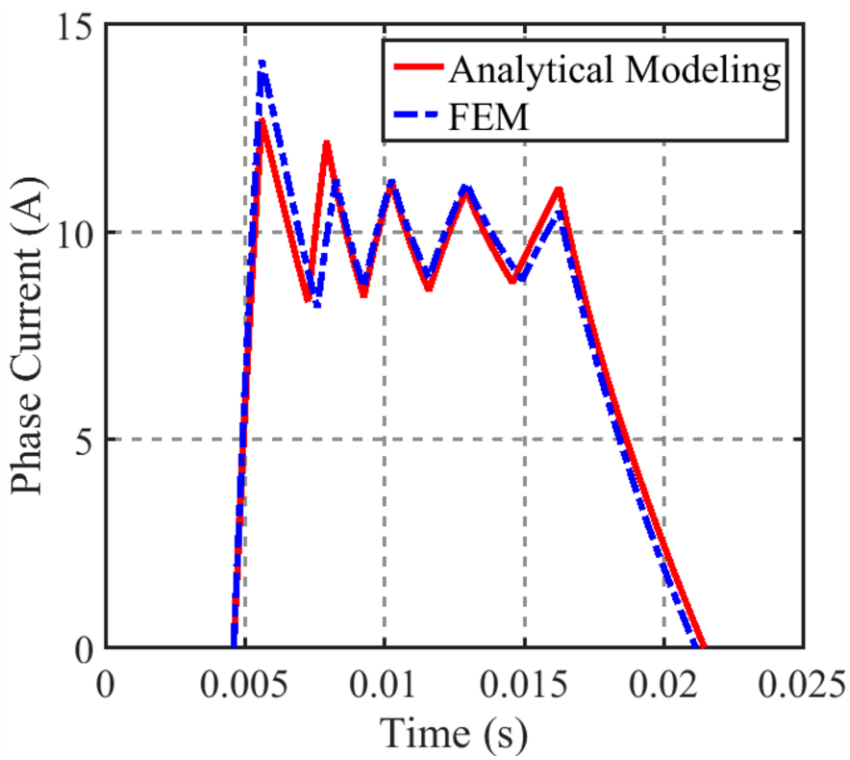

Fig. 16. Instantaneous current waveforms for LSRM

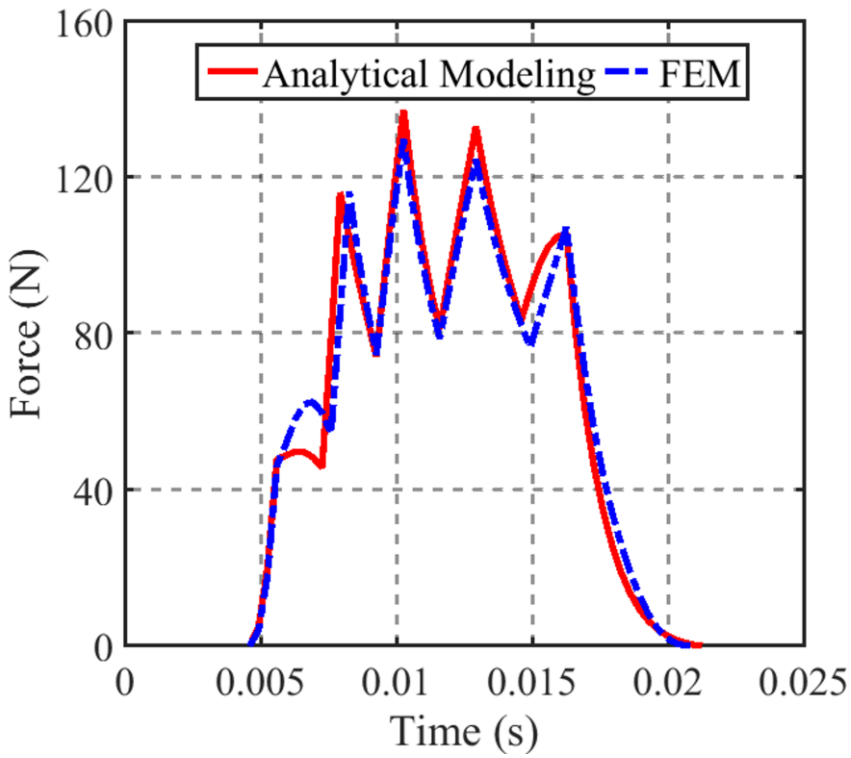

Fig. 17. Instantaneous thrust force waveforms for LSRM

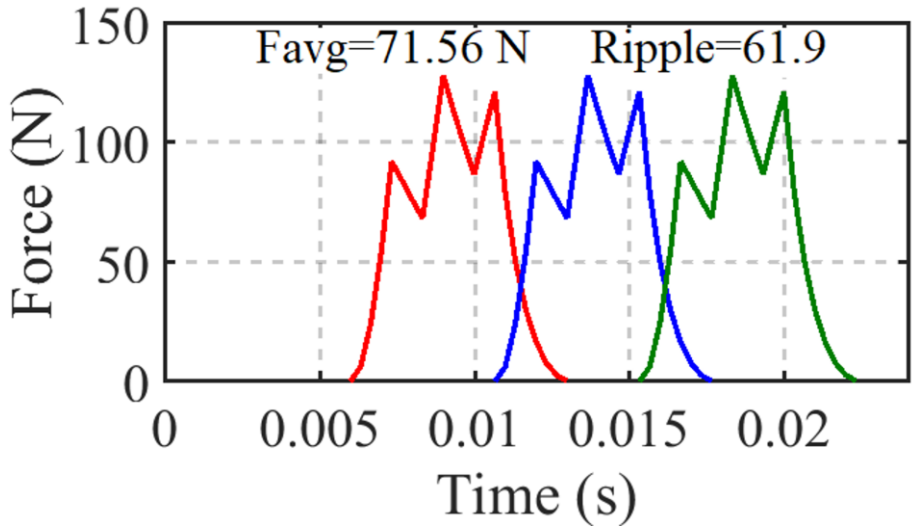

a

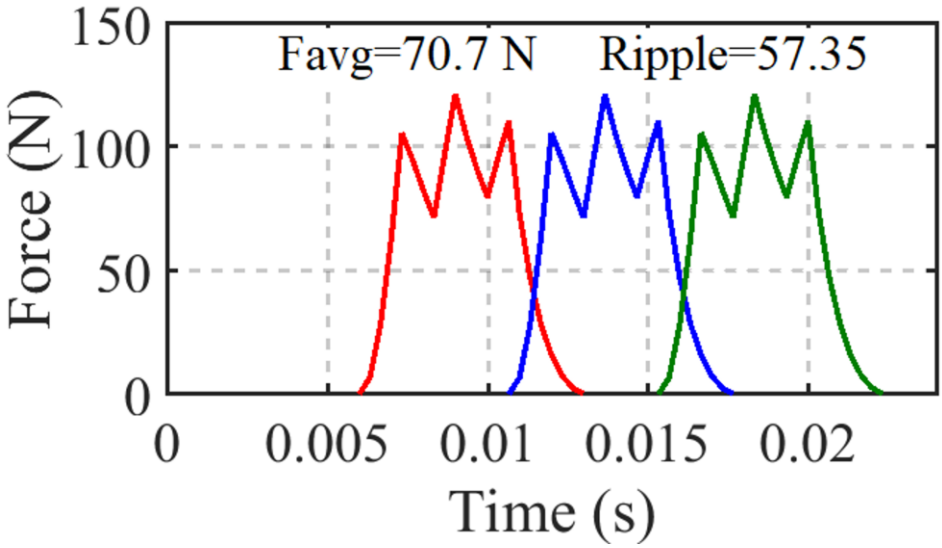

b

Fig. 18. Instantaneous thrust waveforms for the 3-phase LSRM: (a) proposed analytical model, (b) FEM

TABLE 1. SPECIFICATIONS OF THE LSRM

Parameters	Value
Stator pole width [mm]	46
Stator slot width [mm]	46
Stator pole height [mm]	67
Stator yoke height [mm]	46
Air-gap length [mm]	1
Translator pole width [mm]	49
Translator slot width [mm]	89
Translator yoke height [mm]	49
Core stack thickness [mm]	125
Turns per phase	160

TABLE 2. THE FLUX LINKED VALUES (WB.TURNS) FOR SOME TRANSLATOR POSITIONS

Position	Simulation	Current[A]			
		2	6	10	14
Unaligned position	Modeling	0.016	0.048	0.079	0.111
	FEM	0.017	0.050	0.083	0.117
	Error	-5.8%	-4%	-4.8%	-5.1%
Intermediate position	Modeling	0.088	0.259	0.423	0.572
	FEM	0.084	0.251	0.422	0.589
	Error	-4.7%	3.2%	0.24%	-2.9%
Aligned position	Modeling	0.191	0.564	0.915	1.224
	FEM	0.186	0.572	0.969	1.273
	Error	-2.7%	-1.4%	-5.6%	-3.8%

Technical Biography of Authors:

Milad Golzarzadeh received the Ph.D. degree in electrical power engineering from Sharif University of Technology, Tehran, Iran in 2024. His research interests include modeling and design of electrical machines, especially linear switched reluctance motors, thermal modeling of electrical machines, permanent magnet motors, power electronics and drives.

Zahra Nasiri-Gheidari (Senior Member of IEEE) received the B.Sc. degree from Iran University of Science and Technology, Tehran, Iran, in 2004, and the M.Sc. and Ph.D. degrees from University of Tehran, Tehran, in 2006 and 2012, respectively, all in Electrical Engineering. She is currently a Full Professor with the Department of Electrical Engineering, Sharif University of Technology, Tehran, Iran. Her research interests include design, optimization, and performance analysis of electrical machines and electromagnetic sensors.

Hashem Oraee (Fellow of IET, Senior Member of IEEE) received the B.Eng. in electrical and electronic engineering from University of Wales, Cardiff, U.K., in 1980, and the Ph.D. degree in electrical machines from the University of Cambridge, Cambridge, U.K., in 1984. He is currently a Full Professor with the Department of Electrical Engineering, Sharif University of Technology, Tehran, Iran. His current research interests include renewable energies, electrical machines, and DFIGs.

Babak Ganji (Senior Member of IEEE) received the B.Sc. degree from Esfahan University of Technology, Iran in 2000, and M.Sc. and Ph.D. from the University of Tehran, Iran in 2002 and 2009 respectively, all in electrical power engineering. He is currently an Associate Professor with the Faculty of Electrical and Computer Engineering, University of Kashan, Kashan, Iran. His research interest is modeling and design of advanced electrical machines, especially switched reluctance motor.